Purity of (28)Si-Enriched Silicon Material Used for the Determination of the Avogadro Constant

Purity of ^{28}Si-Enriched Silicon Material Used for the Determination of the Avogadro Constant

Giancarlo D'Agostino[1]*, Marco Di Luzio[1-2], Giovanni Mana[1], Massimo Oddone[2], John W. Bennett[3], and Attila Stopic[3]

1 Istituto Nazionale di Ricerca Metrologica (INRIM), Strada delle Cacce 91, 10135 Torino, Italy

2 Department of Chemistry, University of Pavia, via Taramelli 12, 27100 Pavia, Italy

3 Australian Nuclear Science and Technology Organisation (ANSTO), New Illawarra Road, Lucas Heights, NSW 2234, Australia

ABSTRACT: At present, counting atoms in a one-kilogram sphere made of ^{28}Si-enriched silicon allows the determination of the Avogadro constant with the 2.0×10^{-8} relative standard uncertainty required for the realization of the definition of the new kilogram. With the exception of carbon, oxygen, boron, nitrogen and hydrogen, the claimed uncertainty is based on the postulation that the silicon material used to manufacture the sphere was above a particular level of purity. Two samples of the silicon were measured using instrumental neutron activation analysis to collect experimental data to test the purity assumption. The results obtained in two experiments carried out using different research reactor neutron sources are reported. The analysis confirmed that the silicon material was of sufficient purity by quantifying the ultra-trace concentration of 12 elements and determining the detection limits of another 54 elements.

Recently, the X-ray crystal density (XRCD) method used to determine the Avogadro constant, N_A, by counting the atoms in a ^{28}Si-enriched single crystal achieved the target relative standard uncertainty of 2.0×10^{-8} required for the realisation of the new definition of the unit of mass based on the Planck constant, h.[1]

The experiment is performed using a ^{28}Si-enriched single crystal kilogram artefact shaped as a quasi-perfect sphere, whose mass, m, and volume, V, of the silicon core, i.e. not including the surface layers, are accurately measured. The Avogadro constant is given by $N_A = n M V / m a^3$, where $n = 8$ is the number of atoms per unit cell, and M and a are the atomic weight and lattice parameter of the ^{28}Si-enriched crystal, respectively. The M and a values are obtained from samples of the ^{28}Si-enriched boule, called AVO28, that was used to manufacture the sphere.

Since M refers only to the ^{28}Si, ^{29}Si and ^{30}Si mole fractions[2,3], m must be corrected for crystal defects such as impurity atoms and vacancies. As well, these crystal defects change the atom distances according to the individual binding conditions, i.e. the lattice parameter and, as a consequence, the sphere diameter. Though, the effect on the number of unit cells that make up the kilogram artefact, V / a^3, may be compensated for, provided that any variation of the concentration of the defects between the sphere and the sample used to measure a are corrected for.

The latest N_A determination included the corrections due to silicon crystal vacancies and contamination of carbon, oxygen, boron and nitrogen. The amounts of these impurity atoms were measured by means of infrared spectroscopy[4,5] and the amount of vacancies was measured by means of positron lifetime spectroscopy.[6] With the exception of hydrogen[7], the purity with respect to the remaining elements of the periodic table was assumed to be acceptable on the basis of literature data concerning the elemental characterisation of silicon materials produced by the semiconductor industry. It was recognised, however, that experimental evidence to support this assumption would endorse the claimed 2.0×10^{-8} N_A standard uncertainty.

Instrumental neutron activation analysis (INAA) has been widely adopted for the determination of impurities in silicon materials. Advantages of the method are that it is non-destructive, thus avoiding the need to dissolve the sample, and that the activation properties of silicon isotopes (explained below) are such that the detection limit for most detectable elements sits in the ultra-trace range. Through a joint agreement, the Istituto Nazionale di Ricerca Metrologica (INRIM) and the Australian Nuclear Science and Technology Organisation (ANSTO) carried out preliminary tests with samples of natural and ^{28}Si-enriched materials. The results confirmed the possibility of reaching mass fraction detection limits below 1×10^{-9} for a large number of elements.[8-10]

Based on the results of the preliminary tests, the National Metrology Institutes participating in the International Avogadro Coordination (IAC) to determine the Avogadro constant agreed to use the AVO28 material for purity investigations by INAA. This paper presents the details of the neutron activation experiments and reports the results of the measurements.

Determination of the impurities. INAA is a well-established analytical chemistry method for solid sample elemental analysis. It is based on the activation of naturally-occurring nuclides with neutrons and the detection of γ-emissions from the induced radionuclides using high-resolution germanium detectors and spectrometers.

In this study, INAA was performed using the k_0-method of standardisation for most elements and the relative method of standardisation for a few others. In the relative method, the sample and a multi-elemental standard containing known

amounts of the elements of interest are co-irradiated and successively counted. In the k_0-method, a mono-elemental standard containing a known amount of a monitor element is used.

Fundamentals of neutron activation analysis and a description of the two standardisation methods can be found in literature.[11,12] The measurement equations are discussed in detail elsewhere[12] and set out here for reader convenience.

The relative method. In the case of the relative method, the mass fraction $w(^i\mathrm{E})$ of an isotope $^i\mathrm{E}$ of the element of interest, E, in a sample is determined using

$$w(^i\mathrm{E}) = \frac{C^{\mathrm{smp}}_{\gamma_{\mathrm{R}(^i\mathrm{E})}}}{C^{\mathrm{std}}_{\gamma_{\mathrm{R}(^i\mathrm{E})}}} \frac{m_{\mathrm{std,E}}\, x_{\mathrm{smp}}(^i\mathrm{E})}{m_{\mathrm{smp}}} \times \frac{G^{\mathrm{std}}_{\mathrm{th}} f + G^{\mathrm{std}}_{\mathrm{ep}} Q_{0,^i\mathrm{E}}(\alpha)}{G^{\mathrm{smp}}_{\mathrm{th}} f + G^{\mathrm{smp}}_{\mathrm{ep}} Q_{0,^i\mathrm{E}}(\alpha)} \frac{\varepsilon^{\mathrm{std}}_{\mathrm{p},\gamma_{\mathrm{R}(^i\mathrm{E})}}}{\varepsilon^{\mathrm{smp}}_{\mathrm{p},\gamma_{\mathrm{R}(^i\mathrm{E})}}}, \tag{1}$$

where $C^{\mathrm{smp}}_{\gamma_{\mathrm{R}(^i\mathrm{E})}}$ and $C^{\mathrm{std}}_{\gamma_{\mathrm{R}(^i\mathrm{E})}}$ are the count rates of the γ-photons emitted by the radionuclide $\mathrm{R}(^i\mathrm{E})$ produced by $^i\mathrm{E}$, $\gamma_{\mathrm{R}(^i\mathrm{E})}$, in the sample and in the standard at the end of the irradiation, m_{smp} is the mass of the sample, $m_{\mathrm{std,E}}$ is the mass of E in the standard, $x_{\mathrm{smp}}(^i\mathrm{E})$ is the isotopic abundance of $^i\mathrm{E}$ in the sample, f is the thermal to epithermal neuron flux ratio, $Q_{0,^i\mathrm{E}}(\alpha)$ is the resonance integral to 2200 ms^{-1} neutron cross section ratio of $^i\mathrm{E}$ for a $1/E^{1+\alpha}$ epithermal neutron flux, $G^{\mathrm{smp}}_{\mathrm{th}}$, $G^{\mathrm{std}}_{\mathrm{th}}$, $G^{\mathrm{smp}}_{\mathrm{ep}}$ and $G^{\mathrm{std}}_{\mathrm{ep}}$ are the sample and standard correction factors accounting for the thermal and epithermal neutron self-shielding, and $\varepsilon^{\mathrm{smp}}_{\mathrm{p},\gamma_{\mathrm{R}(^i\mathrm{E})}}$ and $\varepsilon^{\mathrm{std}}_{\mathrm{p},\gamma_{\mathrm{R}(^i\mathrm{E})}}$ are the sample and standard full-energy γ-peak detection efficiency of $\gamma_{\mathrm{R}(^i\mathrm{E})}$ corrected for γ-attenuation. The count rates in equation (1) are

$$C_\gamma = \frac{N_{\mathrm{p},\gamma}}{(t_{\mathrm{c}} - t_{\mathrm{dead}})\, k_{\mathrm{coi}}} \frac{1}{D\,C}, \tag{2}$$

where $N_{\mathrm{p},\gamma}$ is the number of counts in the full-energy γ-peak, k_{coi} is the pulse losses factor (random and true coincidence), t_{c} is the counting time, t_{dead} is the absolute dead-time of the detection system, and $D = e^{-\lambda t_{\mathrm{d}}}$ and $C = (1 - \mathrm{e}^{-\lambda t_{\mathrm{c}}})/\lambda t_{\mathrm{c}}$ are decay and counting factors of the produced radionuclide R; t_{d} is the decay time and $\lambda = \ln(2)/t_{1/2}$ is the decay constant of R, given its half-life $t_{1/2}$. For simplicity of notation, here and hereafter the superscripts smp, std and the subscript $\mathrm{R}(^i\mathrm{E})$ are occasionally omitted.

The lowest uncertainty is typically achieved when sample and standard have similar geometry, volume and matrix, and are counted in a distant and equal position with respect to the detector. In this case equation (1) simplifies to

$$w(^i\mathrm{E}) = \frac{C^{\mathrm{smp}}_{\gamma_{\mathrm{R}(^i\mathrm{E})}}}{C^{\mathrm{std}}_{\gamma_{\mathrm{R}(^i\mathrm{E})}}} \frac{m_{\mathrm{std,E}}\, x(^i\mathrm{E})}{m_{\mathrm{smp}}}. \tag{3}$$

The k_0-method. In the case of the k_0 method

$$w(^i\mathrm{E}) = \frac{C^{\mathrm{smp}}_{\mathrm{s},\gamma_{\mathrm{R}(^i\mathrm{E})}}}{F_{\mathrm{c,Au}}} \frac{x_{\mathrm{smp}}(^i\mathrm{E})}{m_{\mathrm{smp}}} \frac{1}{k_{0,\mathrm{Au}}(^i\mathrm{E},\gamma_{\mathrm{R}(^i\mathrm{E})})} \times \frac{1}{G^{\mathrm{smp}}_{\mathrm{th}} f + G^{\mathrm{smp}}_{\mathrm{ep}} Q_{0,^i\mathrm{E}}(\alpha)} \frac{1}{\varepsilon^{\mathrm{smp}}_{\mathrm{p},\gamma_{\mathrm{R}(^i\mathrm{E})}}}, \tag{4}$$

where $k_{0,\mathrm{Au}}(^i\mathrm{E},\gamma_{\mathrm{R}(^i\mathrm{E})}) = \dfrac{M_{\mathrm{Au}}\, x_{\mathrm{std}}(^i\mathrm{E})\, \sigma_{0,^i\mathrm{E}}\, P_{\gamma_{\mathrm{R}(^i\mathrm{E})}}}{M_{\mathrm{E}}\, x_{\mathrm{std}}(^{197}\mathrm{Au})\, \sigma_{0,^{197}\mathrm{Au}}\, P_{\gamma_{198}\mathrm{Au}}}$, is the k_0 factor of the comparator isotope ^{197}Au versus $^i\mathrm{E}$ for the $\gamma_{\mathrm{R}(^i\mathrm{E})}$ emission and

$$F_{\mathrm{c,Au}} = \frac{C^{\mathrm{std}}_{\mathrm{s},\gamma_{\mathrm{R}(^i\mathrm{M})}}}{m_{\mathrm{std,M}}} \frac{1}{k_{0,\mathrm{Au}}(^i\mathrm{M},\gamma_{\mathrm{R}(^i\mathrm{M})})} \times \frac{1}{G^{\mathrm{std}}_{\mathrm{th}} f + G^{\mathrm{std}}_{\mathrm{ep}} Q_{0,^i\mathrm{M}}(\alpha)} \frac{1}{\varepsilon^{\mathrm{std}}_{\mathrm{p},\gamma_{\mathrm{R}(^i\mathrm{M})}}} \tag{5}$$

is the comparator factor. Explicitly, M_{Au} and M_{E} are the molar masses of Au and E, $\sigma_{0,^i\mathrm{E}}$ and $\sigma_{0,^{197}\mathrm{Au}}$ are the 2200 ms^{-1} neutron capture cross sections of $^i\mathrm{E}$ and ^{197}Au, $P_{\gamma_{\mathrm{R}(^i\mathrm{E})}}$ and $P_{\gamma_{198}\mathrm{Au}}$ are the absolute gamma emission probabilities of $\gamma_{\mathrm{R}(^i\mathrm{E})}$ and $\gamma_{198}\mathrm{Au}$. Moreover, $k_{0,\mathrm{Au}}(^i\mathrm{M},\gamma_{\mathrm{R}(^i\mathrm{M})})$ in equation (5) is the k_0 factor of the comparator isotope ^{197}Au versus $^i\mathrm{M}$ for the $\gamma_{\mathrm{R}(^i\mathrm{M})}$ emission, where $^i\mathrm{M}$ is an isotope of the monitor element M, $\gamma_{\mathrm{R}(^i\mathrm{M})}$ is the γ-photon emitted by the radionuclide $\mathrm{R}(^i\mathrm{M})$ produced by $^i\mathrm{M}$; $C^{\mathrm{smp}}_{\mathrm{s},\gamma_{\mathrm{R}(^i\mathrm{E})}}$ and $C^{\mathrm{std}}_{\mathrm{s},\gamma_{\mathrm{R}(^i\mathrm{M})}}$ in equations (4) and (5), respectively, are the saturated count rates of $\gamma_{\mathrm{R}(^i\mathrm{E})}$ and $\gamma_{\mathrm{R}(^i\mathrm{M})}$ corrected for burn-up effects, i.e. $C_{\mathrm{s},\gamma} = \dfrac{C_\gamma}{k_{\mathrm{bu}}\, S}$, with k_{bu}, the burn-up factor and $S = 1 - \mathrm{e}^{-\lambda t_{\mathrm{irr}}}$, the saturation factor of the produced radionuclide R after an irradiation time t_{irr}.

The $k_{0,\mathrm{Au}}$ and Q_0 have been experimentally determined for more than 400 γ-lines emitted by more than 122 radionuclides. The recommended values and the related nuclear data are available.[13]

Some effects such as the possible temporal and spatial neutron flux variations during irradiation or the branching activation and the mother-daughter decay concerning specific target isotopes have been omitted in equations (1) and (4) for simplicity reasons.

Neutron activation of silicon. Silicon is an ideal material for trace element analysis by INAA because silicon isotopes have low neutron activation cross sections and produce relatively short-lived radionuclides.

Specifically, the main neutron capture reactions are ^{28}Si(n,p)^{28}Al, ^{29}Si(n,p)^{29}Al and ^{30}Si(n,γ)^{31}Si. The most intense γ-emissions due to ^{28}Al ($t_{1/2}$ = 2.2 min), ^{29}Al ($t_{1/2}$ = 6.6 min) and ^{31}Si ($t_{1/2}$ = 157.3 min) are 1778.9 keV, 1273.3 keV and 1266.2 keV, respectively. Traces of ^{24}Na ($t_{1/2}$ = 15 h) with γ-emissions at 1368.6 keV and 2754.0 keV are produced by ^{28}Si

through the neutron capture reaction ^{28}Si(n,αp)^{24}Na. Furthermore, previous experiments showed ultra-traces of ^{28}Mg ($t_{1/2}$ = 20.9 h) with γ-emission at 1342.2 keV most likely due to ^{29}Si(n,2p)^{28}Mg and the following γ-emission at 1778.9 keV due to its ^{28}Al daughter.

In the case of a ^{28}Si-enriched material, production of ^{29}Al and ^{31}Si is minimised and the silicon activity is hence limited to the production of ^{28}Al. Thus, after about 20 min from the end of the neutron irradiation, the measurement of contaminant elements is almost free from matrix interference.

EXPERIMENTAL SECTION

To reach the minimum detection limit for the largest number of elements, the neutron activation was carried out using the 20 MW OPAL research reactor operated by ANSTO and the 250 kW TRIGA Mark II reactor operated by the University of Pavia.

Planning the measurements drew on previous experiences[14], where it is recommended among other things use of the highest available irradiation neutron fluxes and most efficient gamma ray detectors. While measurements of high purity silicon have been carried out in many laboratories in the past, mainly to serve the electronic semiconductor industry, measurement of the shorter-lived isotopes does not appear to have been attempted and in some cases was discouraged due to likely interference from ^{31}Si itself (particularly its high β-emission rate and associated gamma spectrometric challenges) resulting in detection limits being too high.

Based on the results of preliminary tests carried out with a ^{28}Si-enriched material, the k_0-method was applied by ANSTO in Australia using short- and long-term neutron irradiations with the aim of quantifying possible contaminant elements. The relative method was applied by INRIM in Italy in an experiment designed for a medium-term neutron irradiation and developed to obtain detection limits for selected contaminant elements using fast neutron reactions. In the latter case, the silicon sample was counted in a non-conventional orientation and the resulting large uncertainty was tolerated to reach the smallest detection limits.

Materials. Two identical cylindrical silicon samples, identified as Si28-10-Pr11 part 6.9.2 and Si28-10-Pr11 part 6.9.3, hereafter called S1 and S2, respectively, were used in this work. A picture of the samples is shown in figure 1.

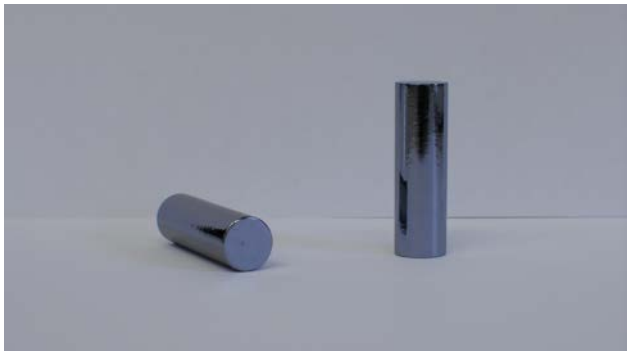

Figure 1. The two samples of the ^{28}Si-enriched cut from the AVO28 crystal.

They were cut by the Physikalisch Technische Bundesanstalt (PTB) from the ^{28}Si-enriched AVO28 crystal produced within the IAC project. After cutting, the mass, m, diameter, ϕ, and length, l, of the crystals were 5.2 g, 9.6 mm and 31.1 mm, respectively.

Silicon sample S1 was selected for the experiment in Australia and silicon sample S2 for the experiment in Italy. To eliminate the surface contamination due to silicon machining, about 80 μm of material, i.e. 0.2 g, was removed by etching the samples for 20 min in isotropic etch (10:1 of nitric acid, HNO_3, assay 67-69%, and hydrofluoric acid, HF, assay 47-51%).

Two samples, 2 mm length and 3.7 mg mass, of Al-0.1%Au wire (IRMM-530R, 1 mm diameter) and one sample, approximately 70 mm length and 38 mg mass, of Al-0.1%Co wire (IRMM-527R, 0.5 mm diameter) were cut and used as mono-elemental standards (Au and Co monitors) for the k_0-method. Five elemental solutions, 1000 μg mL^{-1} Pb, Tl, Ti and 10000 μg mL^{-1} Ni, Nb (AlfaAesar, Specpure®), were used to prepare the multi-elemental standards for the relative method.

Several polyethylene (PE) vials and a high purity Al foil (Sigma-Aldrich #356859, 50 μm thickness) were utilised for the neutron irradiation of the standards and silicon samples.

The etching container, the tweezers used to handle the silicon samples and the irradiation vials were cleaned in an ultrasonic bath with 10% nitric acid. The water was purified using a Millipore system (ρ > 18 MΩ cm) and the chemicals were of ultrapure grade.

Short-term Irradiation Experiment. The S1 sample and the two Al-0.1%Au wires were weighed with an electromagnetic balance calibrated with SI-traceable weights and sealed in three PE vials for the short-term experiment.

The neutron irradiation lasted 10 min and was performed in the NAA-SRT facility which is a 'fast-access' pneumatic irradiation position in the OPAL reactor (nominal thermal neutron flux, Φ_{th} = 2.2 × 10^{13} cm^{-2} s^{-1}, thermal to epithermal neutron flux ratio f = 3250, α = 0.15). The silicon sample and the Al-0.1%Au wires were closed in a PE irradiation can and sent to the reactor using a pneumatic transfer system. The two Al-0.1%Au wires were located above and below the silicon sample (see figure 2a).

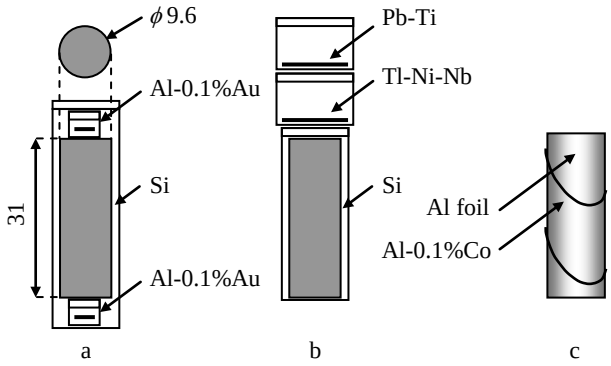

Figure 2. The relative position of the silicon sample and standards during (a) the short-term neutron irradiation, (b) the medium-term neutron irradiation and (c) the long-term neutron irradiation. Dimensions are in mm.

After irradiation, the silicon sample was removed from its vial and measured. Three γ-spectra were sequentially collected with a high purity germanium (HPGe) detector, ORTEC GEM35-70-PL (58 mm crystal diameter, 39 % relative efficiency, 1.69 keV FWHM resolution at 1332 keV) inside a low-background graded lead shield. The acquisition of the first γ-spectrum, ST1, started at $t_{d\,ST1}$ = 13.6 min and lasted $t_{c\,ST1}$ = 6.0 min. Next, the silicon

sample was cleaned in an ultrasonic bath with de-ionised water. The acquisition of the second and third γ-spectrum, ST2 and ST3, started at $t_{d\,ST2}$ = 20.9 min and $t_{d\,ST3}$ = 61.7 min, and lasted $t_{c\,ST2}$ = 7.8 min and $t_{c\,ST3}$ = 22.7 h, respectively. The spectrometry was performed in zero dead-time mode, i.e. t_{dead} = 0 min.

The 411.8 keV ^{198}Au γ-emission of the two Al-0.1%Au wires was measured with a HPGe detector ORTEC GEM25P4-PLUS (59 mm crystal diameter, 32 % relative efficiency, 1.67 keV FWHM resolution at 1332 keV).

The acquisition of the first γ-spectrum, Au1, started at $t_{d\,Au1}$ = 3.12 h and lasted $t_{c\,Au1}$ = 1.11 h. The acquisition of the second γ-spectrum, Au2, started at $t_{d\,Au2}$ = 4.84 h and lasted $t_{c\,Au2}$ = 1.39 h; both were performed in zero dead-time mode.

The detectors were connected to ORTEC DSPEC-Pro digital spectrometers, and the data were collected using a personal computer running the ORTEC Maestro® software.[15]

The position of the S1 sample and of the Al-0.1%Au wire with respect to the detector end-cap is shown in figure 3a and figure 3b, respectively.

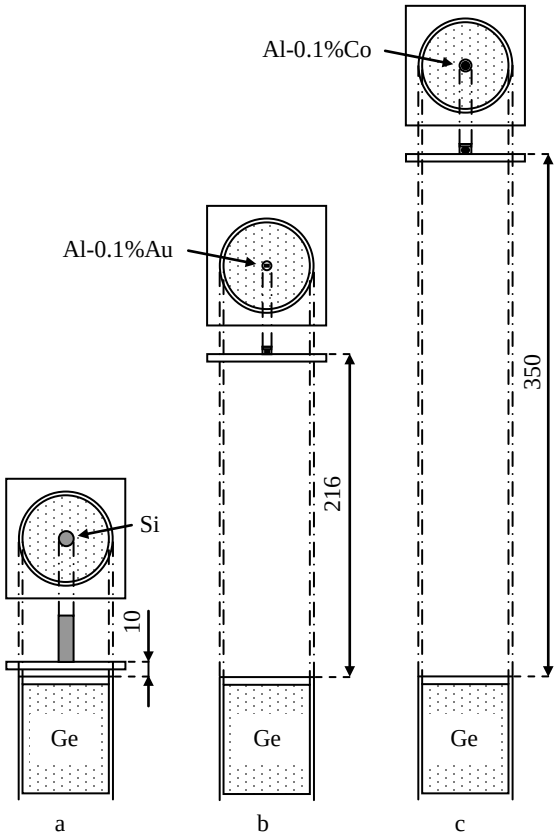

Figure 3. The γ-counting position of (a) the S1 silicon sample, (b) the Al-0.1%Au wire and (c) the Al-0.1%Co wire with respect to the detector end-cap. Dimensions are in mm.

Medium-term Irradiation Experiment. Two multi-elemental standards, Pb-Ti and Tl-Ni-Nb, were prepared for the medium-term experiment by pipetting aliquots of the standard solutions in two PE vials weighed with an electromagnetic balance calibrated with SI-traceable weights. Before sealing, the pipetted solutions were dried out using an infrared lamp.

The neutron irradiation lasted 6 h and was performed in the central channel of the TRIGA Mark II reactor (fast neutron flux with neutron energy E > 100 keV, $\Phi_{fast} = 6.8 \times 10^{12}$ cm^{-2} s^{-1}). The silicon sample and the multi-elemental standards were closed in a PE can and manually placed in the reactor. The two multi-elemental standards were located above the silicon sample (see figure 2b).

At the end of the irradiation, the silicon sample was removed from its vial, etched (HNO_3 / HF 10:1) for 30 s, weighed and measured. Two γ-spectra were sequentially collected. The acquisition of the first γ-spectrum, MT1, started at $t_{d\,MT1}$ = 6.1 h and lasted $t_{c\,MT1}$ = 20.0 h with a negligible dead-time. The acquisition of the second γ-spectrum, MT2, started at $t_{d\,MT2}$ = 113.6 h and lasted $t_{c\,MT2}$ = 70.9 h with a negligible dead-time.

The multi-elemental standards were consecutively measured. The acquisition of the Pb-Ti γ-spectrum, MS1, started at $t_{d\,MS1}$ = 80.7 h and lasted $t_{c\,MS1}$ = 11.4 h with a $t_{dead\,MS1}$ = 8 min. The acquisition of the Tl-Ni-Nb γ-spectrum, MS2, started at $t_{d\,MS2}$ = 103.1 h and lasted $t_{c\,MS2}$ = 2.6 h with $t_{dead\,MS2}$ = 6 min.

The γ-photons were detected with an HPGe detector ORTEC GEMS8530P4 (85 mm crystal diameter, 50 % relative efficiency, 1.90 keV FWHM resolution at 1332 keV) inside a low-background graded lead shield. The ORTEC DSPEC jr 2.0 digital spectrometer and ORTEC Gamma Vision® software[16] were used for data processing and acquisition.

The position of the S2 sample and of the multi-elemental standards with respect to the detector end-cap is shown in figure 4a and figure 4b, respectively.

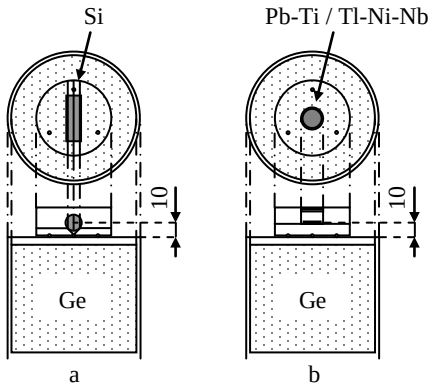

Figure 4. The γ-counting position of (a) the S2 silicon sample and (b) the Pb-Ti and Tl-Ni-Nb standards with respect to the detector end-cap. Dimensions are in mm.

Long-term Irradiation Experiment. After 54 days from the end of the short-term irradiation, the S1 sample was prepared for the long-term irradiation experiment. The silicon was weighed and enveloped in the high purity Al foil. Next, the Al-0.1%Co wire was weighed and spiral wrapped around the sample (see figure 2c).

The neutron exposure lasted 120 h and was performed in the LE6-1C channel of the OPAL reactor ($\Phi_{th} = 6.5 \times 10^{13}$ cm^{-2} s^{-1}, f = 262, α = 0.143). The silicon sample and the monitor were placed in an aluminium can and sent to the reactor vessel with a pneumatic transfer system. Higher neutron fluxes are available in other pneumatic irradiation channels in OPAL, namely in LE7 which is approximately 1×10^{14} cm^{-2} s^{-1}. However LE6 was chosen because the neutron spectrum is significantly better thermalised there (f = 44 in LE7), and it was expected that the better thermalised channel with the slightly lower flux would largely eliminate interferences from epithermal and fast neutron reactions.

In order to apply the measurement model (4) with the commonly adopted definition of saturation factor *S*, the neutron flux during a long irradiation is assumed to be stable. However, OPAL is a busy multi-purpose reactor that is automatically controlled to maintain constant thermal power as targets are inserted/extracted and fuel burns up, with the consequence that the neutron flux may vary significantly over a 5 day irradiation. To check whether a more complicated form of S was needed, a neutron flux profile was obtained from data logged at 5 min intervals over the course of the long irradiations using two of the reactor's nucleonic channels (compensated ion chambers) located at the edge of the OPAL reflector vessel.

After the irradiation, the Al-0.1%Co wire was removed from the silicon sample, wound into a 5 mm diameter spherical shape and placed in a counting PE vial. The aluminium foil was removed and the silicon sample was cleaned in an ultrasonic bath with acetone. The silicon sample was measured by collecting four γ-spectra with the ORTEC GEM35-70-PL detector. The acquisition of the first γ-spectrum, LT1, started at $t_{\mathrm{d\,LT1}} = 97.7$ h and lasted $t_{\mathrm{c\,LT1}} = 11.1$ h with $t_{\mathrm{dead\,LT1}} = 6$ min. Next, the silicon sample was etched (HNO_3 / HF 10:1) for 3 min and weighed again. The acquisition of the second and third γ-spectrum, LT2 and LT3, started at $t_{\mathrm{d\,LT2}} = t_{\mathrm{d\,LT3}} = 243$ h, and lasted $t_{\mathrm{c\,LT2}} = 20.4$ h and $t_{\mathrm{c\,LT3}} = 165$ h, respectively, with $t_{\mathrm{dead\,LT2}} = 7.5$ min and $t_{\mathrm{dead\,LT3}} = 44$ min. The acquisition of the fourth γ-spectrum, LT4, started at $t_{\mathrm{d\,LT4}} = 1351$ h and lasted $t_{\mathrm{c\,LT4}} = 281$ h with negligible dead-time.

The 1173.2 keV and 1332.5 keV ^{60}Co γ-emission of the Al-0.1%Co wire was measured with the HPGe detector ORTEC GEM35-70-PL. The acquisition of the γ-spectrum started at $t_{\mathrm{d\,Co}} = 144$ h and lasted $t_{\mathrm{c\,Co}} = 13.3$ min with $t_{\mathrm{dead\,Co}} = 2.8$ min.

The position of the silicon sample and of the Al-0.1%Co wire with respect to the detector is shown in figure 3a and figure 3c, respectively.

RESULTS AND DISCUSSION

The application of the k_0-method allowed, via equation (4), to quantify the mass fraction, $w(^i\mathrm{E})$, of 12 elements and to determine a mass detection limit for 49 elements.

The recorded spectra of the silicon sample and of the monitors were processed using Hyperlab® software[17] to determine the number of counts, $N_{\mathrm{p},\gamma}$, at every full-energy γ-peak of any measurable radionuclide. In the absence of a γ-peak, $N_{\mathrm{p},\gamma}$ is replaced by the detection limit according to Currie's method[18,19] using a background region centred at the γ-peak energy and a width equivalent to 3 FWHM at that energy.

The resulting peak table files were input into Kayzero for Windows® software[20] to calculate $w(^i\mathrm{E})$, apart from Ir which was calculated manually due to the software not yet incorporating the new k_0 factors for ^{192}Ir. In the case of an isotope quantified with more than one γ-peak, the weighted average value was reported, while, in the case of a non-quantified isotope, the lowest detection limit was taken as a final result.

The data were corrected for neutron self-shielding, pulse losses and burn-up. In detail, since the self-shielding of the monitors is negligible, $G_{\mathrm{th}}^{\mathrm{std,Au}} = G_{\mathrm{ep}}^{\mathrm{std,Au}} = G_{\mathrm{th}}^{\mathrm{std,Co}} = G_{\mathrm{ep}}^{\mathrm{std,Co}} = 1$. In addition, given the cylindrical dimensions and isotopic composition of the silicon sample, $G_{\mathrm{th}}^{\mathrm{smp}} = 0.989$ and $G_{\mathrm{ep}}^{\mathrm{smp}} = 1.000$.[21] The full-energy γ-peak detection efficiencies of the sample included the geometry and γ-attenuation corrections. The main contribution to the lost pulses was the true coincidence; pulse loss factors ranged between 0.824 and 1.012, for the ^{175}Yb 396.3 keV and the ^{82}Br 776.6 keV γ-emissions, respectively. Finally, the burn-up effect was significant only for ^{197}Au and ^{191}Ir and the correction factors 0.764 and 0.965 were applied, respectively.

All results determined using the k_0-method used the simple form of the saturation faction *S* (constant flux) as the neutron flux was found to be stable enough for the duration of the irradiation. To double check this, *S* was also calculated using the variable flux method for the shortest-lived radionuclide measured from this irradiation, i.e. ^{187}W, which represented the worst case in terms of differences between the methods (longer-lived radionuclides would be less affected). The difference between the results obtained with constant flux and variable flux saturation factors was 0.09 %, which was considered low enough to not necessitate the additional computations the variable flux method would require.

Few spectral interference corrections needed to be made. The most significant correction concerned the 1120.5 keV γ-emission due to ^{46}Sc from the silicon crystal and ^{214}Bi background from the shielding, where the majority of the counts in the peak was found to be coming from the background. No fast neutron activation products were detected in any of the long-lived measurements, including the oft-mentioned ^{24}Na which is usually present in such samples as a result of the ^{28}Si(n,αp)^{24}Na reaction. This result highlights how well thermalised the neutron spectrum was at the irradiation position.

Only a single element, Mn, was quantified after the short-term irradiation. Detection limits for Na, Mg, Al, Cl, K, V, Ge, Y, Rh, In, Sn, I, Dy and Er were calculated for these elements that produce shorter-lived radionuclides. Normally, the significant β-emission from ^{31}Si in natural silicon greatly increases the background of γ-spectra due to Bremsstrahlung for hours after the irradiation, resulting in poorer detection limits. In this case the effect is significantly limited by the fact that the enriched silicon sample was so depleted in ^{30}Si. Detection limits for Ti, Ni and Nb were also determined using (n,γ) reactions, ^{50}Ti(n,γ)^{51}Ti ($t_{1/2}$ = 5.8 min), ^{64}Ni(n,γ)^{65}Ni ($t_{1/2}$ = 2.5 h) and ^{93}Nb(n,γ)^{694m}Nb ($t_{1/2}$ = 6.3 min). However, the use of longer-lived threshold reactions ^{47}Ti(n,p)^{47}Sc ($t_{1/2}$ = 3.3 d), ^{58}Ni(n,p)^{58}Co ($t_{1/2}$ = 71 d) and ^{93}Nb(n,2n)^{92m}Nb ($t_{1/2}$ = 10 d) in the medium-term irradiation experiment resulted in lower detection limits.

The long-term irradiation experiment produced detection limits comparable to other similar measurements performed elsewhere using similar techniques. Incidentally, this is possibly the first application of iridium measurement using the k_0 method using the isotope ^{192}Ir, which has demonstrated the superior sensitivity over ^{194}Ir which was previously the only isotope usable by k_0-NAA users.[13]

The uncertainty of the quantified mass fractions is essentially due to counting statistics, positioning and geometry correction of the silicon sample. The overall contribution of the latter two depends on a positioning tolerance of about of ± 1 mm and is evaluated to be about 4 %. The knowledge of the remaining parameters, including the k_0 and Q_0 values[13] has minor effect on the results. Concerning the detection limits, the uncertainty is conservatively evaluated to be at 10 % level.

The application of the relative method, via equation (1), allowed mass fraction detection limits to be determined for Ti, Ni, Nb, Tl and Pb.

Table 1. A summary of the impurity content in samples of the AVO28 material in terms of quantified or detection limit mass fraction, w(E),and number density, N(E). The neutron capture reaction, the half-life of the produced radionuclide, $t_{1/2}$, the isotopic abundance, $x(^i\text{E})$, the energy of the detected γ-peak and the selected γ-spectrum are also reported. The detection limits are evaluated according to Currie's method and the uncertainties (k = 1) in parentheses apply to the last respective digits. Spectrometric measurements which were carried out before post-irradiation etching are marked with *. Unless otherwise specified, the adopted $t_{1/2}$, $x(^i\text{E})$ and energy of the γ-peak are taken from the database of recommended k_0-data.[13]

Reaction	$t_{1/2}$	$x(^i\text{E})$	γ-peak / keV	γ-spectrum	w(E) / g g^{-1}	N(E) / cm^{-3}
^{23}Na(n,γ)^{24}Na [a]	14.96 h	1.0000	1368.6	ST2	$\leq 1.0 \times 10^{-10}$	$\leq 6.1 \times 10^{12}$
^{26}Mg(n,γ)^{27}Mg	9.462 min	0.1101	843.8	ST2	$\leq 1.7 \times 10^{-8}$	$\leq 9.9 \times 10^{14}$
^{27}Al(n,γ)^{28}Al [b]	2.2414 min	1.0000	1778.9	ST1	$\leq 5.0 \times 10^{-6}$	$\leq 2.6 \times 10^{17}$
^{37}Cl(n,γ)^{38}Cl	37.24 min	0.2423	2167.4	ST1	$\leq 2.8 \times 10^{-10}$	$\leq 1.1 \times 10^{13}$
^{41}K(n,γ)^{42}K	12.36 h	0.0673	1524.7	ST3	$\leq 8.6 \times 10^{-10}$	$\leq 3.1 \times 10^{13}$
^{46}Ca(n,γ)^{47}Sc	3.349 d	0.000035	159.4	LT3	$\leq 2.6 \times 10^{-9}$	$\leq 9.2 \times 10^{13}$
^{45}Sc(n,γ)^{46}Sc	83.83 d	1.0000	889.3	LT3	$2.46(38) \times 10^{-14}$	$0.76(12) \times 10^{9}$
^{47}Ti(n,p)^{47}Sc	3.349 d	0.0744 [22]	159.4	MT2	$\leq 4.3 \times 10^{-9}$	$\leq 1.2 \times 10^{14}$
^{51}V(n,γ)^{52}V	3.75 min	0.9975	1434.1	ST2	$\leq 4.8 \times 10^{-10}$	$\leq 1.3 \times 10^{13}$
^{50}Cr(n,γ)^{51}Cr	27.7 d	0.0435	320.1	LT3	$2.26(11) \times 10^{-10}$	$6.07(30) \times 10^{12}$
^{55}Mn(n,γ)^{56}Mn	2.579 h	1.0000	846.8	ST3*	$4.75(32) \times 10^{-12}$	$1.208(81) \times 10^{11}$
^{58}Fe(n,γ)^{59}Fe	44.5 d	0.0028	1099.3, 1291.6	LT3	$8.53(49) \times 10^{-10}$	$2.13(12) \times 10^{13}$
^{59}Co(n,γ)^{60}Co	1925.3 d	1.0000	1173.2, 1332.5	LT3	$1.190(80) \times 10^{-12}$	$2.82(19) \times 10^{10}$
^{58}Ni(n,p)^{58}Co	70.86 d [22]	0.0068 [22]	810.7 [22]	MT2	$\leq 6.8 \times 10^{-10}$	$\leq 1.6 \times 10^{13}$
^{63}Cu(n,γ)^{64}Cu	12.7 h	0.6917	1345.8	LT1	$\leq 1.9 \times 10^{-9}$	$\leq 4.2 \times 10^{13}$
^{64}Zn(n,γ)^{65}Zn	244.3 d	0.4860	1115.5	LT3	$5.46(30) \times 10^{-11}$	$1.167(64) \times 10^{12}$
^{71}Ga(n,γ)^{72}Ga	14.1 h	0.3990	834.0	LT1	$\leq 1.0 \times 10^{-11}$	$\leq 2.0 \times 10^{11}$
^{74}Ge(n,γ)^{75}Ge	82.78 min	0.3650	139.7	ST3	$\leq 1.1 \times 10^{-8}$	$\leq 2.0 \times 10^{14}$
^{75}As(n,γ)^{76}As	26.24 h	1.0000	559.1	LT1*	$2.52(27) \times 10^{-12}$	$4.70(50) \times 10^{10}$
^{74}Se(n,γ)^{75}Se	119.781 d	0.0089	136.0	LT4	$\leq 2.0 \times 10^{-12}$	$\leq 3.5 \times 10^{10}$
^{81}Br(n,γ)^{82}Br	35.3 h	0.4931	776.5	LT1*	$8.04(34) \times 10^{-12}$	$1.406(59) \times 10^{11}$
^{85}Rb(n,γ)^{86}Rb	18.63 d	0.7217	1077.0	LT4	$\leq 7.2 \times 10^{-12}$	$\leq 1.2 \times 10^{11}$
^{84}Sr(n,γ)^{85}Sr	64.84 d	0.0056	514.0	LT3	$\leq 1.0 \times 10^{-10}$	$\leq 1.7 \times 10^{12}$
^{89}Y(n,γ)^{90m}Y	3.19 h	1.0000	202.5	ST3	$\leq 2.6 \times 10^{-8}$	$\leq 4.1 \times 10^{14}$
^{94}Zr(n,γ)^{95}Nb	34.97 d	0.1728	765.8	LT4	$\leq 1.4 \times 10^{-12}$	$\leq 2.1 \times 10^{10}$
^{93}Nb(n,2n)^{92m}Nb	10.15 d [22]	1.0000	934.4 [22]	MT2	$\leq 3.6 \times 10^{-8}$	$\leq 5.5 \times 10^{14}$
^{98}Mo(n,γ)^{99m}Tc	6.01 h	0.2413	140.5	LT1	$\leq 1.4 \times 10^{-11}$	$\leq 2.1 \times 10^{11}$
^{102}Ru(n,γ)^{103}Ru	39.35 d	0.3160	497.1	LT3	$\leq 9.3 \times 10^{-13}$	$\leq 1.3 \times 10^{10}$
^{103}Rh(n,γ)^{104}Rh	42.3 s	1.0000	555.8	ST1	$\leq 3.0 \times 10^{-9}$	$\leq 4.0 \times 10^{13}$
^{108}Pd(n,γ)^{109}Ag	39.6 s	0.2646	88.0	LT1	$\leq 3.1 \times 10^{-10}$	$\leq 4.1 \times 10^{12}$
^{109}Ag(n,γ) ^{110m}Ag	249.8 d	0.4817	657.8	LT4	$\leq 1.2 \times 10^{-12}$	$\leq 1.5 \times 10^{10}$
^{114}Cd(n,γ) ^{115m}In	4.486 h	0.2872	336.2	LT1	$\leq 1.8 \times 10^{-11}$	$\leq 2.2 \times 10^{11}$
^{115}In(n,γ)^{116m}In	54.41 min	0.9570	1293.5	ST3	$\leq 1.0 \times 10^{-13}$	$\leq 1.2 \times 10^{9}$
^{122}Sn(n,γ)^{123}Sn	40.06 min	0.0460	160.3	ST3	$\leq 2.0 \times 10^{-10}$	$\leq 2.3 \times 10^{12}$
^{121}Sb(n,γ)^{122}Sb	2.724 d	0.5730	564.2	LT3	$1.61(12) \times 10^{-12}$	$1.85(14) \times 10^{10}$
^{123}Sb(n,γ)^{124}Sb	60.2 d	0.4270	602.7	LT3	$1.49(10) \times 10^{-12}$	$1.71(11) \times 10^{10}$
^{130}Te(n,γ)^{131}I	8.021 d	0.3380	364.5	LT4	$\leq 3.9 \times 10^{-12}$	$\leq 4.3 \times 10^{10}$
^{127}I(n,γ)^{128}I	24.99 min	1.0000	442.9	ST2	$\leq 9.6 \times 10^{-11}$	$\leq 1.1 \times 10^{12}$
^{133}Cs(n,γ)^{134}Cs	2.065 y	1.0000	604.7	LT4	$\leq 2.3 \times 10^{-13}$	$\leq 2.4 \times 10^{9}$
^{130}Ba(n,γ)^{131}Ba	11.5 d	0.00106	496.3	LT3	$\leq 5.8 \times 10^{-11}$	$\leq 5.9 \times 10^{11}$
^{139}La(n,γ) ^{140}La	1.678 d	0.9991	1596.2	LT3	$\leq 1.7 \times 10^{-12}$	$\leq 1.7 \times 10^{10}$
^{140}Ce(n,γ) ^{141}Ce	32.51 d	0.8848	145.4	LT3	$\leq 1.2 \times 10^{-12}$	$\leq 1.2 \times 10^{10}$
^{141}Pr(n,γ) ^{142}Pr	19.12 h	1.0000	1575.6	LT1	$\leq 1.9 \times 10^{-11}$	$\leq 1.9 \times 10^{11}$
^{146}Nd(n,γ)^{147}Nd	10.98 d	0.1719	91.1	LT3	$\leq 3.0 \times 10^{-12}$	$\leq 2.9 \times 10^{10}$
^{152}Sm(n,γ)^{153}Sm	46.5 h	0.2660	103.2	LT1	$\leq 5.4 \times 10^{-14}$	$\leq 5.0 \times 10^{8}$
^{151}Eu(n,γ) ^{152}Eu	13.54 y	0.4786	121.8	LT4	$\leq 3.8 \times 10^{-14}$	$\leq 3.5 \times 10^{8}$
^{152}Gd(n,γ)^{153}Gd	240.4 d	0.0020	97.4	LT4	$\leq 4.1 \times 10^{-12}$	$\leq 3.7 \times 10^{10}$
^{159}Tb(n,γ)^{160}Tb	72.3 d	1.0000	298.6	LT4	$\leq 1.3 \times 10^{-13}$	$\leq 1.1 \times 10^{9}$
^{164}Dy(n,γ)^{165}Dy	2.334 h	0.2810	94.7	ST3	$\leq 2.2 \times 10^{-12}$	$\leq 1.9 \times 10^{10}$
^{165}Ho(n,γ)^{166}Ho	26.83 h	1.0000	80.6	LT1	$\leq 8.5 \times 10^{-13}$	$\leq 7.2 \times 10^{9}$
^{170}Er(n,γ)^{171}Er	7.516 h	0.1490	308.3	ST3	$\leq 6.2 \times 10^{-11}$	$\leq 5.2 \times 10^{11}$
^{169}Tm(n,γ)^{170}Tm	128.6 d	1.0000	84.3	LT4	$\leq 4.4 \times 10^{-13}$	$\leq 3.6 \times 10^{9}$
^{174}Yb(n,γ)^{175}Yb	4.185 d	0.3183	396.3	LT3	$\leq 1.3 \times 10^{-13}$	$\leq 1.0 \times 10^{9}$
^{176}Lu(n,γ)^{177}Lu	6.73 d	0.0259	208.4	LT3	$\leq 5.1 \times 10^{-14}$	$\leq 4.1 \times 10^{8}$
^{174}Hf(n,γ)^{175}Hf	70 d	0.00163	343.4	LT4	$\leq 1.6 \times 10^{-13}$	$\leq 1.2 \times 10^{9}$

Reaction	$t_{1/2}$	$x(^{i}\mathrm{E})$	γ-peak / keV	γ-spectrum	$w(\mathrm{E})$ / g g^{-1}	$N(\mathrm{E})$ / cm^{-3}
^{181}Ta(n,γ)^{182}Ta	114.4 d	0.9999	67.8	LT4	$\leq 2.2 \times 10^{-13}$	$\leq 1.7 \times 10^{9}$
^{186}W(n,γ)^{187}W	23.72 h	0.2864	685.7	LT1*	$2.53(34) \times 10^{-12}$	$1.92(26) \times 10^{10}$
^{185}Re(n,γ)^{186}Re	3.718 d	0.3740	137.2	LT3	$\leq 1.4 \times 10^{-13}$	$\leq 1.1 \times 10^{9}$
^{190}Os(n,γ)^{191}Os	15.4 d	0.2640	129.4	LT3	$\leq 3.0 \times 10^{-13}$	$\leq 2.2 \times 10^{9}$
^{191}Ir(n,γ)^{192}Ir	73.827 d	0.3730	308.5, 316.5, 468.1	LT3	$7.18(96) \times 10^{-15}$	$5.22(70) \times 10^{7}$
^{198}Pt(n,γ)^{199}Au	3.139 d	0.0720	158.4	LT3	$\leq 8.7 \times 10^{-12}$	$\leq 6.2 \times 10^{10}$
^{197}Au(n,γ)^{198}Au	2.695 d	1.0000	411.8	LT2	$1.004(64) \times 10^{-13}$	$7.12(45) \times 10^{-8}$
^{202}Hg (n,γ)^{203}Hg	46.61 d	0.2970	279.2	LT2	$\leq 1.4 \times 10^{-12}$	$\leq 9.7 \times 10^{9}$
^{203}Tl(n,2n)^{202}Tl	12.31 d [22]	0.29524 [22]	439.5 [22]	MT2	$\leq 3.7 \times 10^{-8}$	$\leq 2.5 \times 10^{14}$
^{204}Pb(n,2n)^{203}Pb	51.92 h [22]	0.014 [22]	279.2 [22]	MT1	$\leq 5.6 \times 10^{-7}$	$\leq 3.8 \times 10^{15}$
^{232}Th(n,γ)^{233}Pa	26.97 d	1.0000	311.9	LT3	$\leq 7.9 \times 10^{-14}$	$\leq 4.7 \times 10^{8}$
^{238}U(n,γ)^{239}Np	2.357 d	0.9928	106.1	LT1	$\leq 1.4 \times 10^{-12}$	$\leq 8.2 \times 10^{9}$

a) Possible interference with ^{28}Si(n,αp)^{24}Na, b) Interference with ^{28}Si(n, p)^{28}Al

The number of counts in the full-energy γ-peak, $N_{\mathrm{p},\gamma}$, were extracted from the collected spectra of the multi-elemental standards using the fitting algorithm of the Gamma Vision® software. The detection limits were manually calculated from the spectra of the silicon sample using Currie's method and 3 FWHM background width.

Since the multi-elemental standards and the axis of the silicon sample are located at 10 mm from the detector end-cap (see figure 4a and figure 4b), the unity value is assigned to the sample and standard efficiency ratio in equation (1). A positioning tolerance of ± 2 mm is expected, which corresponds to about ± 25 % variation of the full-energy γ-peak detection efficiency. The contribution to the uncertainty of the remaining parameters, e.g. the masses and the count rates, is minor and the self-shielding and pulse losses correction factors are set to the unity value with negligible consequence. Thus, taking into account also the neutron flux gradient at the irradiation position and the effect of different γ-attenuation and geometries, the detection limit values are affected by an uncertainty up to a few tens of per cent.

The results of the neutron activation experiments are listed in table 1.

The quantified or the detection limit mass fraction of E, $w(\mathrm{E})$, and the corresponding number density of E, $N(\mathrm{E})$, are obtained from equations (1) and (4). In addition, the neutron capture reaction, the half-life of the produced radionuclide, the isotopic abundance, the detected γ-peak and the selected γ-spectrum are reported.

General remarks. In principle, different sources of contamination of the AVO28 material are possible, starting from silicon dioxide selected for the first decomposition step to the final floating zone growth of the ^{28}Si-enriched boule, including the step of the ^{28}Si-enrichment of gaseous SiF_4.

Although the isotope enrichment acts as a chemical purification step, the isotopic composition of the impurity elements of the final material could differ from the natural one, specifically for those contaminant elements that can be transformed into gaseous chemical compounds and are subjected to the centrifugal separations during the enrichment step.

However, since there is no experimental evidence of this effect, the natural isotopic abundances reported in table 1 are adopted to compute the amount of the contaminants. Furthermore, it should be noted that in this study the quantified Sb in AVO28 has a natural isotopic composition because the concentration of Sb obtained from the ^{121}Sb and ^{123}Sb isotopes are in independent agreement.

CONCLUSIONS

A panoramic analysis of impurities in the ^{28}Si-enriched crystal produced to determine the Avogadro constant has been carried out using instrumental neutron activation analysis at two research reactors. On the basis of the results obtained in this study, the widely accepted assumption of crystal purity has been experimentally confirmed with respect to a large number of possible contaminant elements.

Specifically, the content of Fe, Cr and Zn was quantified to be $8.53(49) \times 10^{-10}$ g g^{-1}, $2.26(11) \times 10^{-10}$ g g^{-1} and $5.46(30) \times 10^{-11}$ g g^{-1}, respectively; uncertainties ($k = 1$) in parentheses apply to the last respective digits. Also Sc, Ir and Au were quantified with mass fractions within the range 10^{-15} g g^{-1} and 10^{-13} g g^{-1} and Mn, Co, As, Br, Sb and W with mass fractions at the 10^{-12} g g^{-1} level. Several elements including Mn, As, Br and W could only be quantified prior to post-irradiation etching. Previous experience has shown that the contamination of outer layer of the silicon sample is possible, so the concentration of these elements in the bulk of the crystal will most likely be much lower than the reported values.

Assuming that the quantified contaminants are associated with interstitial lattice sites and that the gradients of their concentration along the AVO28 boule is negligible, the corresponding mass deficit, m_{deficit}, i.e. difference between the mass of a kilogram sphere having Si atoms occupying all the regular sites and the measured mass core value[1], is -1.154(50) μg.

Additionally, no trace of Ga, Se, Rb, Zr, Ru, Ag, In, Te, Cs, La, Ce, Nd, Sm, Eu, Gd, Tb, Di, Ho, Tm, Yb, Lu, Hf, Ta, Re, Os, Pt, Hg, Th and U was found to within 1.0×10^{-11} g g^{-1}. Detection limits from 1.0×10^{-11} g g^{-1} to 1.0×10^{-8} g g^{-1} were reached for Na, Cl, K, Ca, Ti, V, Ni, Cu, Sr, Mo, Rh, Pb, Cd, Sn, I, Ba, Pr and Er, and from 1.0×10^{-8} g g^{-1} to 5.0×10^{-6} g g^{-1} for Mg, Al, Ge, Y, Nb, Tl and Pb.

AUTHOR INFORMATION

Corresponding Author

*E-mail: g.dagostino@inrim.it

Notes

The authors declare no competing financial interest.

ACKNOWLEDGMENTS

This work was jointly funded by the European Metrology Research Programme (EMRP) participating countries within the European Association of National Metrology Institutes (EURAMET), the European Union, and the Italian ministry of education, university, and research (awarded project P6-2013,

implementation of the new SI). The authors would like to thank the PTB workshop for cutting AVO28 crystals and H. Bettin for valuable discussions and technical support.

REFERENCES

(1) Azuma, Y.; et al. *Metrologia* **2015**, *52*, 360-375.

(2) Pramann, A.; Rienitz, O.; Noordmann, J.; Güttler, B.; Schiel, D. *Z. Phys. Chem.* **2014**, *228*, 405-419.

(3) D'Agostino, G.; Di Luzio, M.; Mana, G.; Oddone, M.; Pramann, A.; Prata, M. *Anal. Chem.* **2015**, *87*, 5716-5722.

(4) B Andreas, B.; et al. *Metrologia* **2011**, *48*, S1-S13.

(5) Itoh, Y.; Nozaki, T.; Masui, T.; Abe, T. *Phys. Lett.* **1985**, *47*, 488-489.

(6) Krause-Rehberg, R. *Laboratory Report* University Halle-Wittenberg, Germany **2008**.

(7) Lavrov, E. 2010 *Laboratory Report* University of Technology Dresden, Germany **2010**.

(8) D'Agostino, G.; Bergamaschi, L.; Giordani, L.; Mana, G.; Oddone, M. *Metrologia* **2012**, *49*, 696-701.

(9) D'Agostino, G.; Bergamaschi, L.; Giordani, L.; Mana, G.; Oddone, M. *J. Radioanal. Nucl. Chem.* **2014**, *299*, 277-282.

(10) Nawara, W. Australian Nuclear Science and Technology Organisation, Lucas Heights, Australia, Unpublished work, 2013

(11) Greenberg, R.; Bode, P.; De Nadai Fernandes, E. A. *Spectrochim. Acta B* **2011**, *66*, 193-241.

(12) De Corte, F. *Habilitation Thesis* University of Gent, Belgium **1987**.

(13) *Database of recommended k_0-data* released 11.1.2016 by k_0-Nuclear Data Subcommittee of k_0-International Scientific Committee.

(14) Verheijke, ML.; Jaspers, HJJ.; Hanssen, JMG. *J. Radioanal. Nucl. Chem.* **1989**, *131*, 197-214.

(15) Maestro®, *Version 6.0* by Advanced Measurement Technology, Inc.

(16) GammaVision®, *Version 6.08* by Advanced Measurement Technology, Inc.

(17) Hyperlab®, *Version 2013* by Hyperlabs Software.

(18) Currie, L. A. *Anal. Chem.* **1968**, *40*, 586-593.

(19) Bergamaschi, L.; D'Agostino, G.; Giordani, L.; Mana, G.; Oddone, M. *Metrologia* **2013**, *50*, 269-276.

(20) Kayzero for Windows®, *Version 2* by DSM Research.

(21) Chilian, C.; St-Pierre, J.; Kennedy, G. *J. Radioanal. Nucl. Chem.* **2008**, *278*, 745-749.

(22) Chart of Nuclides, National Nuclear Data Center, Brookhaven National Laboratory http://www.nndc.bnl.gov/chart/

Table of Contents graphic